PERGAMON

Computers and Structures 69 (1998) 361–382

Computers & Structures

Basic issues in the finite element simulation of extended end plate connections

O.S. Bursi [a,*], J.P. Jaspart [b]

[a] *Department of Mechanical and Structural Engineering, University of Trento, Via Mesiano 77, 38050 Trento, Italy*
[b] *Department MSM, University of Liège, Quai Banning 6, 4000 Liège, Belgium*

Received 26 May 1997; accepted 28 April 1998

Abstract

Numerical simulations of steel bolted connections performed with finite element models depend heavily upon constitutive relationships, step size, number of integration points, kinematic descriptions, element types and discretizations.

The aforementioned items combined with complex non-linear phenomena which are commonly observed in connections render the finite element technique not attractive for this class of problems. In this paper these issues are scrutinized and both a legitimate methodology suitable to the analysis of extended end plate moment resisting connections and proper three-dimensional finite element models are established. These models are provided first for non-preloaded and preloaded bolted tee stubs which are proposed as benchmarks. Next, both a solid model and an assemblage of three-dimensional beam finite elements, viz. the *spin*, are proposed to model the bolt behaviour either in a rigorous or simplified fashion, respectively. Lastly, a three-dimensional non-linear finite element model suitable for the analysis of isolated extended end plate connections is proposed and validated.

Keywords: Beam-to-column connection; Three-dimensional model; Bolt model; Solid element; Contact element

1. Introduction

The popularity of moment resisting joints with extended connecting end plates can be attributed mainly to the simplicity and economy associated with their design, fabrication and erection. These connections are used frequently to achieve a *rigid* connection behaviour. On the other hand, steel structures need often the lowest level of detailing compatible with design requirements. A solution to this problem is obtained with the recent semi-rigid design philosophy. This approach provides greater freedom than fully-restrained design because the properties of connections are treated as variables in design. The potential economic implication of connections on frame design and fabrication is also realized by modern codes, such as LRFD [1] and Eurocode 3 [2]. As a result, special design guides for moment resisting connections have been developed [3, 4].

Since the aforementioned connection types are highly indeterminate, current design approaches cannot model in a straightforward fashion three-dimensional (3-D) physical systems which are governed by complex combined material and geometrical non-linearities, friction, slippage, contact, bolt-end plate interactions and, eventually, fractures. Hence, the finite element technique has been adopted as a rational supplement to the calibration of design models.

In the current study, the key issues which strive at obtaining an accurate simulation of bolted connections by means of non-linear finite element models are addressed. Thereby, a legitimate methodology is established to calibrate finite element models able to repro-

* Corresponding author.

0045-7949/98/$ - see front matter
PII: S0045-7949(98)00136-9

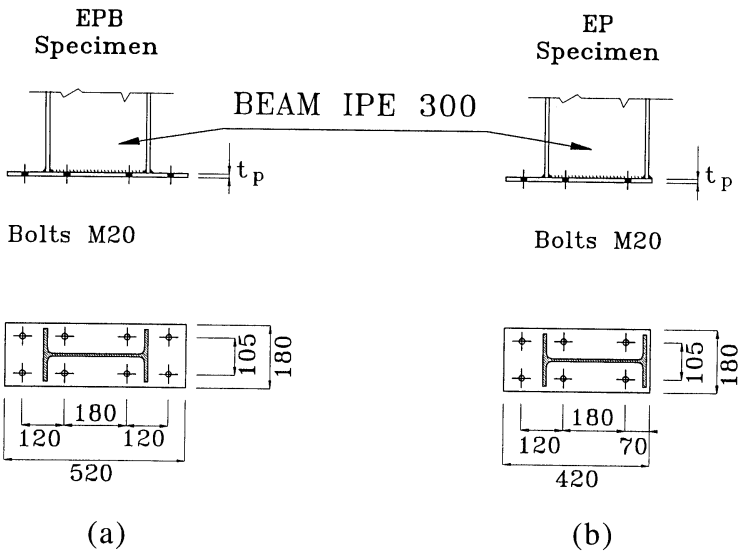

Fig. 1. Geometrical characteristics of tested specimens: (a) EPB connection; (b) EP connection.

duce the elastic–plastic behaviour of bolted connections to post-failure. The comparison between computed and measured values in each phase permits the effectiveness and degree of accuracy of the proposed finite element models to be highlighted. However, no completeness is claimed, and only monotonically increased displacement is considered in this study.

2. Accuracy of design procedures

The characterization of the moment–rotation (M–ϕ) relationship of a bolted connection is a difficult task because the connection response is non-linear over virtually the entire range of loading. To acquire experimental information as well as to verify available design procedures, isolated extended end plate connections, which reflect different geometrical and strength parameters, were tested to collapse under monotonically increased loading [5]. Fig. 1 highlights nomenclature, geometrical characteristics as well as details of the aforementioned connections. Within the EP–EPB specimens, only the thickness value t_p of the connecting end plate is varied to single out the effect of the end plate component. These values are collected in column 2 of Table 1. Beam-to-column fasteners were M 20 grade 8.8 bolts and a preloading force equal to 40% of yield stress was applied to simulate the snug tight condition.

Fig. 2 shows a part of the counterbeam adopted in the set-up to reproduce a very stiff column as well as the ensuing definition of rotation. In detail, for an isolated extended end plate ϕ results from the sum of the flexibilities of end plate and bolts, respectively. Moreover, the same figure illustrates a typical (M–φ) relationship and the basic parameters determined by means of a trilinear approximation. In particular, $K_{e,exp}$ defines the experimental elastic stiffness, $K_{h,exp}$ estimates the strain–hardening stiffness of the moment–rotation law whilst $M_{p,exp}$ defines the plastic failure moment of the connection.

To examine both the degree of accuracy and limitations of codes, the design procedure described in AISC publications [1, 3] and based on the extensive numerical and physical studies carried out by Krishnamurthy [6] was applied to the 14 specimens. By assuming the plastic failure moments $M_{p,exp}$ of each end plate as known quantities (see column 5 of Table 2), end plate thicknesses were reckoned without resistance factors. Actual end plate thicknesses, t_{actual},

Table 1
End plate thicknesses [1]

Specimen	t_{actual} (mm)	$t_{required}$ (mm)
EPB 1–1	12.0	25.0
EPB 2–1	12.0	27.0
EPB 1–2	15.6	26.0
EPB 1–3	18.6	28.0
EPB 1–4	21.8	35.0
EPB 1–5	25.7	37.0
EPB 2–5	25.0	38.0
EP 1–1	12.0	22.0
EP 2–1	12.0	26.0
EP 1–2	15.6	26.0
EP 1–3	18.6	27.0
EP 1–4	21.8	35.0
EP 1–5	25.7	37.0
EP 2–5	25.0	39.0

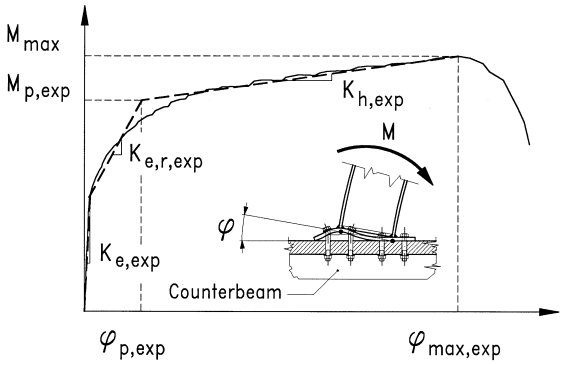

Fig. 2. Rotation definition for an isolated exended end plate joint and $(M-\varphi)$ skeleton relationship with a relevant approximation.

as well as the computed ones, t_{required}, are collected in columns 2 and 3 of Table 1. The discrepancy between the aforementioned thickness values reaches about 50% for thin end plates. It originates mainly from the adoption of the design procedure outside the parameters considered in the original work of Krishnamurthy [6].

As a modern code, Eurocode 3 [2] contains application rules [4] which allow the moment–rotation behaviour of beam-to-column connections to be determined, explicitly. However, for design purposes only the key parameters of the moment–rotation law, viz. the initial elastic stiffness and the design resistance, have to be approximated analytically. Once these quantities are evaluated, a mathematical expression is adopted to reproduce the design $(M–\varphi)$ relationship. Measured $K_{\text{e,exp}}$ and reckoned stiffnesses $K_{\text{e,th}}$ with the respective ratios are collected in columns 2–4 of Table 2. One can observe that the model underestimates the stiffness values for thin end plates, which are characterized by a complex displacement field [7]. However, one must also consider that initial stiffnesses are very sensitive to lack of fit. As a result, discrepancies between experimental stiffness values of similar specimens are expected too. Measured plastic failure moments $M_{\text{p,exp}}$ are also compared to the predicted values $M_{\text{p,th}}$ in columns 5–7 of Table 2. Results show that the design model is on the safe side generally, and that discrepancies are concentrated in thin end plates in which the actual failure mechanisms are effectively 3-D [7]. For subsequent use, the mechanical properties of a connection with a thin end plate, viz. the EP 1–1 connection, are reported in Table 3. In detail, the average tensile values of yield stress f_{y} and ultimate stress f_{u} of different components are collected, respectively.

The aforementioned comparisons between experimental values and code predictions indicate that modern design procedures still need a refinement phase owing to the complex phenomena embodied in bolted connections. In addition, one should consider that the underestimation of both stiffness and strength of connections can be considered on the safe in a static loading regime, but, *a priori*, it is unsafe in a dynamic setting. Hence, the finite element technique is deemed necessary as a rational supplement to the calibration of design procedure.

Latest generation research and commercial finite element codes are capable of simulating almost all complex phenomena which characterize bolted end plate connections. However, some difficulties remain to the numerical analyst which has to choose appropriate models able to provide an accurate representation of the physics with the lowest computational cost. Choice of constitutive law, integration scheme at the constitutive level, number of integration points, step size, kinematic description and discretization depend upon

Table 2
Measured and computed [2] values

Specimen	$K_{\text{e,exp}}$ (kNm/mrad)	$K_{\text{e,th}}$ (kNm/mrad)	$K_{\text{e,th}}/K_{\text{e,exp}}$	$M_{\text{p,exp}}$ (kNm)	$M_{\text{p,th}}$ (kNm)	$M_{\text{p,th}}/M_{\text{p,exp}}$
EPB 1–1	217	58	0.27	94	71	0.75
EPB 2–1	192	65	0.34	96	74	0.77
EPB 1–2	214	105	0.49	148	125	0.84
EPB 1–3	273	146	0.53	166	153	0.92
EPB 1–4	250	170	0.68	183	161*	0.88
EPB 1–5	272	183	0.67	177	179*	1.01
EPB 2–5	203	182	0.90	190	182	0.96
EP 1–1	210	59	0.28	120	96	0.80
EP 2–1	186	55	0.29	98	71	0.72
EP 1–2	215	107	0.50	146	122	0.83
EP1–3	251	137	0.54	156	151	0.97
EP 1–4	277	166	0.60	179	159*	0.89
EP 1–5	318	184	0.58	184	182*	0.99
EP 2–5	231	177	0.77	192	178	0.93

* The design moment resistance is not considered.

Table 3
Characteristics of extended end plate EP 1–1

EP 1–1	t_p Φ (mm)	Yield stress f_y (MPa)	Tensile stress f_u (MPa)
End plate	12.0	321	449
Beam top flange	10.2	256	408
Beam web	6.7	282	425
Beam bottom flange	10.2	249	403
Weld metal	10.0	430	476
Bolt shank	20.0	877	1063

problem, geometry, type of loading and required accuracy.

To shed light on these problems, elementary non-preloaded and preloaded tee stub connections were tested by Bursi and Jaspart [8] and were proposed as benchmarks in the validation process of finite element software packages. These specimens reflect different geometrical and strength parameters as well as bolt prestressing conditions. They are labelled $T1$ and $T2$, but for conciseness, only the specimen $T1$ is analyzed in the remainder of the study. It is shown with its geometrical characteristics in Fig. 3(a) and it was designed purposely to fail according to the collapse mechanism illustrated in Fig. 3(b) [4]. Average tensile values of yield stress f_y and ultimate stress f_u of both flange and web material are collected in Table 4. Fasteners were M 12 grade 8.8 bolts and characterized by the yield and ultimate stress values collected in the same table. Within $T1$ specimens both non-preloaded and preloaded bolts were used. In particular, a prestressing force $S = 60.7$ kN was applied. The characteristics of specimen $T2$ as well as test results and simulations are described and commented upon in [8].

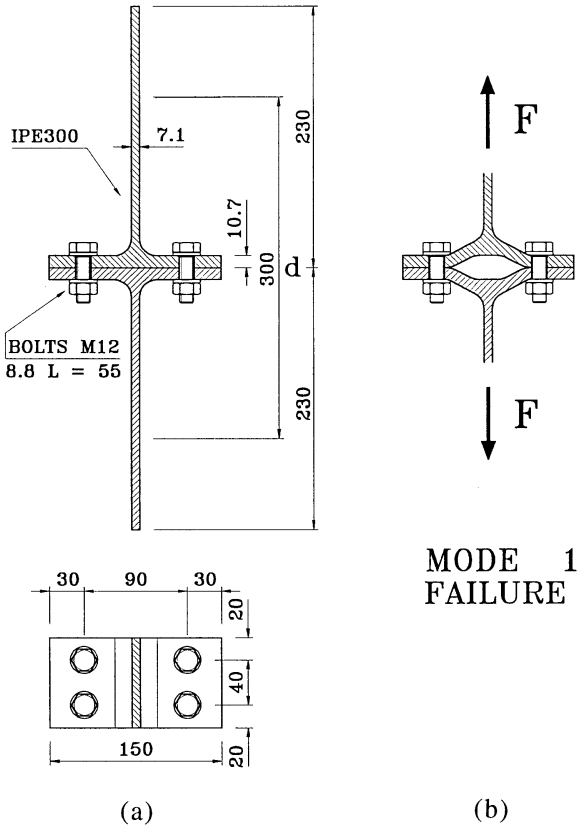

Fig. 3. Test specimens: (a) tee-stub connection $T1$; (b) mode 1 pattern according to Eurocode 3 [2].

3. Non-linear finite element modeling

3.1. State of the art

Krishnamurthy was the pioneer in the field of 3-D modeling of connections, by adopting eight-node subparametric bricks in order to reproduce the behaviour of bolted end plate connections [9]. The analyses carried out were linearly elastic but expensive, because contact was embodied artificially by attaching and releasing nodes at each loading step on the basis of the stress distribution. Bolt preloading phenomena were simulated also. Then, a correlation between two-dimensional (2-D) and 3-D finite element analyses was established and a parametric study was conducted with 2-D models, owing to the limited computer capabilities. A similar procedure was proposed by Kukreti et al. [10] in order to reproduce moment–rotation relationships of end plate connections. The results of these analyses were excellent, albeit they can be used only inside the range for which such validations were performed. However, fundamental issues relating to number of integration points, kinematic description, element type and discretization were not investigated. Kukreti et al. [11] also developed finite element models for stiffened steel tee-hanger connections. These models can be classified as hybrid because they encompassed solid elements for both plates and bolts and plane elements for both web and stiffeners. Satisfactory results were obtained by means of these models though they depend heavily on the used nominal material proper-

Table 4
Characteristics of tee-stub *T*1

Tee-stub *T*1	t_p Φ (mm)	Yield stress f_y (MPa)	Tensile stress f_u (MPa)
Flange	10.7	431	595
Web	7.1	469	591
Bolt shank	12.0	893	974

ties. Nevertheless, some basic issues like discretization and type of yield criterion were faced up.

Since then, other researchers developed 2-D finite element models for bolted connections and, generally, an excellent agreement between analyses and experiments was provided. An enormous effort owing to the general inadequacy of the approach. Indeed, 2-D displacement-based finite element models predict stiffer and stronger solutions compared to the corresponding 3-D models, unless both the connection displacement and stress fields are almost 2-D.

Recently, researchers used 3-D finite element models based either on shell and *separator* truss elements [12] or shell and contact elements [13], in order to simulate end plate as well as beam and column flange behaviour. The agreement between simulations and test data was satisfactory because both contact and beam elements were adopted to simulate friction and bolt action, respectively. But, so far as the simulation of prying forces is concerned, only elements suitable to thick shell analysis can simulate the evolution of internal normal stresses required to satisfy equilibrium with prying forces. Indeed, thin shell elements do not reproduce shear stresses and lead to an overestimation of the plastic failure load.

A rigorous approach to the modeling of bolted connections was adopted later by Gebbeken et al. [14], which discretized bolted tee stubs in a 3-D fashion by means of eight-node brick elements, and investigated the contact problem between deformable bodies in a small deformation regime. Comparisons between simulated and measured data were good. However, the parametric study on end plate joints was performed with 2-D finite element models, thus limiting the analysis effectiveness. In the same light, 3-D finite element models based on solid and contact elements of the ABAQUS library [15, 16] were proposed by Bursi and Leonelli [17] to simulate the rotational behaviour of isolated bolted end plate connections. Numerical results were satisfactory but conditioned strongly by the adoption of one element layer along the end plate thickness.

3.2. Discretization

From the previous section, it is implicit that solid and contact elements could accurately simulate bolted connection behaviour. As a results, they represent the basic elements adopted in the proposed models. To gain insight into the performances of eight-node hexahedron and contact elements as a function of spatial discretization, two simple bending-dominated model problems, namely, a clamped and a simply-supported beam were considered by Li [18].

The comparisons are performed by means of the solid element, *viz*. JET3-D [19], and the benchmark provided by Jetteur and Cescotto [20], which examined the same problem in plain strain with a 2-D element, labeled JET2-D. Each JET3-D element incorporates one Gauss integration point whilst lateral constraints render the 3-D problem a plain-strain problem. The material properties adopted in the simulations are $E = 2 \times 10^5$ N/mm^2, $v = 0.3$, $f_y = 400$ N/mm^2 and a strain–hardening modulus $E^T = 0.1$ N/mm^2. The loading is applied by imposing a deflection at the beam center as shown in Fig. 4(a). The length L of the beam equal to 600 mm is fixed and is discretized by means of 24 elements. The depth, labeled H, is discretized by means of one, two, three, five and eight elements. Two ratios L/H, equal to 10 and 30, are examined, respectively, to capture the slenderness influence. Both the undeformed and deformed beam configurations are shown in Fig. 4(a).

The load–displacement relationships for the two slendernesses are plotted in Fig. 4(b) and (c), respectively. One can observe that the finite element model with one layer provides unacceptable results. The two-layer model appears satisfactory in the elastic regime but provides unsatisfactory results in the inelastic one. All models with more than two layers provide excellent results even in the large displacement regime, in which membrane effects govern the inelastic response.

The meshes relative to the simply-supported beam examined in the simulations are shown in Fig. 5(a). It is long, $L = 34$ mm, and only 21 elements are adopted to discretize half of it. The depth is modelled by one, two, four and six elements whilst two ratios L/H, equal to 10 and 30, are examined, respectively. The boundary conditions are constituted by simple supports of finite length and are simulated by means of contact elements without friction [21]. The corresponding initial and final displacement fields are shown in Fig. 5(a). One can observe the good performance of contact elements. Fig. 5(b) and (c) shows the numerical

simulations in terms of load *vs* displacement for the two slendernesses, $L/H = 10$ and $L/H = 30$, respectively. As far as the beam strength is concerned, one can notice that the one and two-layer finite element models provide inadequate predictions. Thereby, one may conclude that for bending-dominated problems at least three-layers of solid elements have to be used to capture the stiffness and strength behaviour of a structure with good accuracy. However, a two-layer model appears to be adequate for elastic-type analyses in which only the structures initial stiffness is of interest.

3.3. Element types

To minimize the number of assumptions in connection modeling both hexahedra [19] and contact finite elements [21] implemented in the research code LAGAMINE [22] have been adopted. The hexahedron element is much more suitable to model the continuum compared to standard shell elements. Often, 20 nodes (Serendipity brick) or 27 nodes (Lagrangian brick) which can accommodate full triquadratic expansion are adopted. However, to a large extent, the use of one element or the other depends upon the application. In case of elasticity-type (elliptic) problems, much higher solution accuracy per degree of freedom is provided with the higher-order elements. However, for plasticity-type (hyperbolic) problems, in which elements have to reproduce yield lines, *viz*. strain field discontinuities, the first-order elements are likely to be the most successful, because some components of the displacement solution can be discontinuous at element edges. Indeed, the most rigorous approach would require finite elements which admit strain discontinuities in their formulation, to avoid direction and mesh size sensitivity [23]. Nevertheless, these elements are not yet used in general purpose codes because they have not been fully tested. Hence, the eight node hexahedron was also chosen for the numerical simulations of benchmarks because its use implies cheap computations and an easy input.

The brick with eight nodes and full integration (eight Gauss points) could trigger off shear locking. Thereby, an assumed strain field within a mixed-multi-field variational principle able to eliminate spurious energy-modes and a geometry dependent parameter set to control shear locking have been embodied in the JET3-D element [19] of LAGAMINE.

The simulations performed in this study, also adopted three eight-node bricks of the ABAQUS library [15]: (1) The C3D8 element with full integration (8 Gauss points). This element is accurate at the constitutive law integration level, but it can experience the shear locking phenomenon. (2) The C3D8R element with reduced integration (1 Gauss point). This element provides a remedy for shear locking but the rank-deficiency of the stiffness matrix may engender spurious singular (hourglassing) modes. These modes are controlled in the ABAQUS code [16] with the artificial stiffness method proposed by Flanagan and Belytschko [24]. (3) The C3D8I element with full integration (8 Gauss points) and incompatible modes. This element has 13 additional degrees of freedom [25], and it is conceived to eliminate the so-called parasitic shear stresses that are observed in bending-dominated problems.

The contact and distribution of interface stresses between two bodies are unknown during a contact process, and therefore, the contact problem turns out to be highly non-linear and with unknown boundary conditions. This phenomenon is simulated in LAGAMINE by means of contact elements which describe topological surfaces. The contact condition is guaranteed by a penalty technique [21], which requires an optimal value for a penalty parameter. As a result, contact constraints are satisfied only in the limit of an infinite penalty value. Usually, its optimum value is traced if there is only a slight change in the results for an additional increase of the penalty parameter. As an

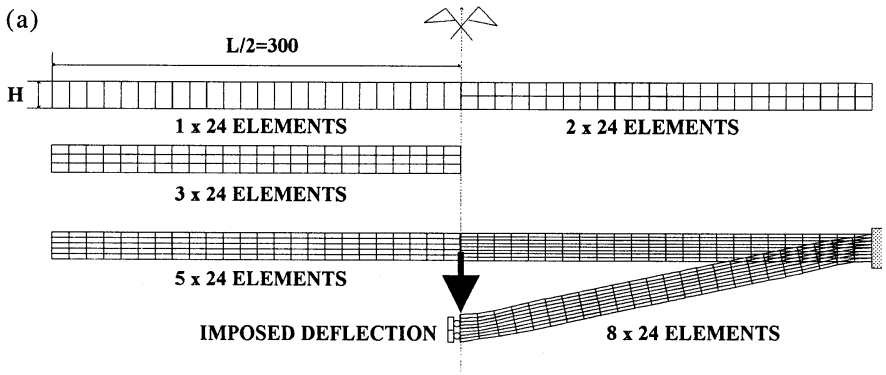

Fig. 4a. *Caption opposite*

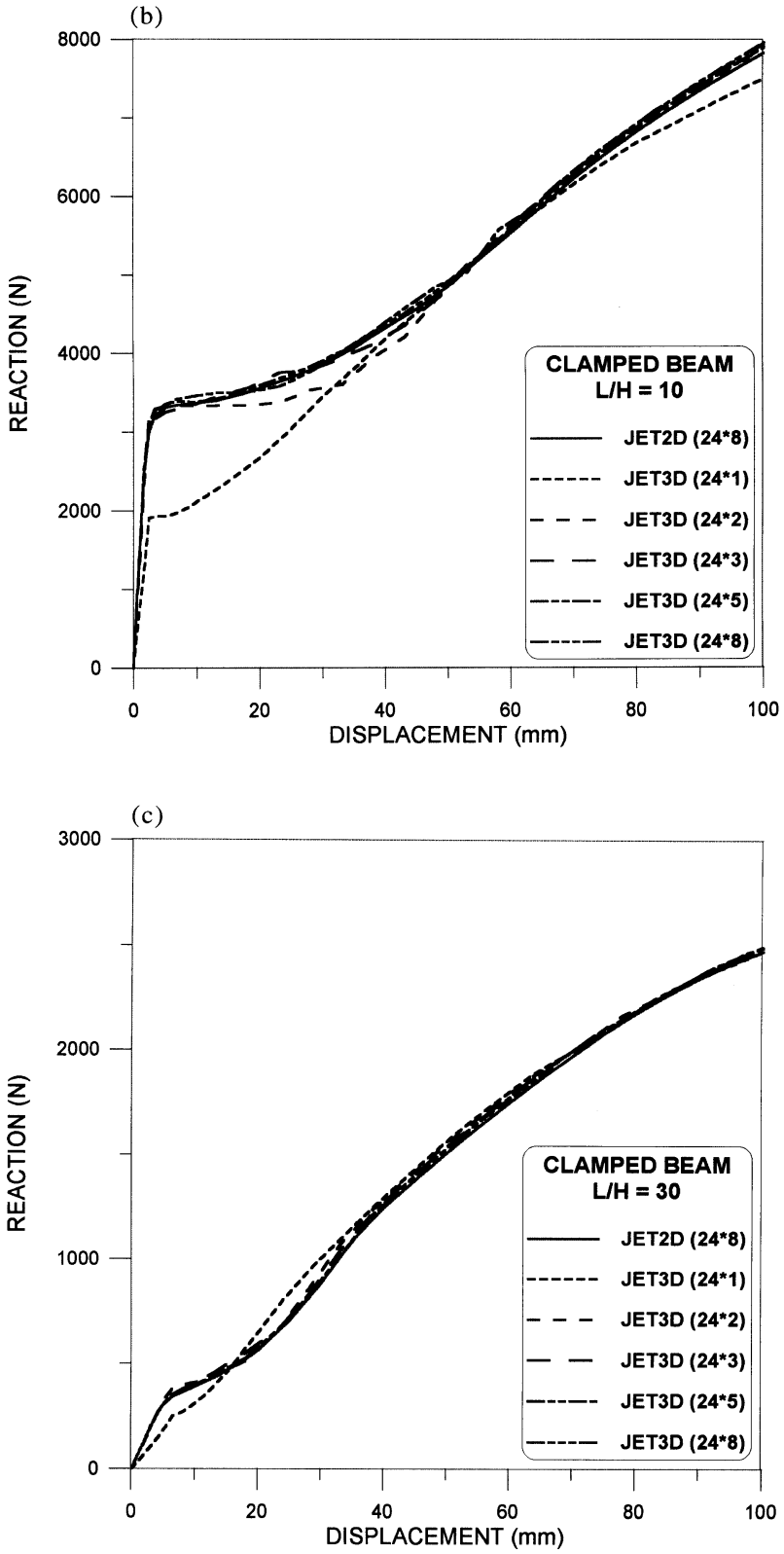

Fig. 4. Clamped beam with an imposed central deflection [18]: (a) FE idealizations; (b) simulations for a slenderness ration $L/H = 10$; (c) simulations for a slenderness ratio $L/H = 30$.

alternative, the contact condition can be enforced exactly by means of Lagrange multiplier techniques, which do not require *a priori* user-defined parameters. The sliding and sticking conditions between bodies have been reproduced with a classical isotropic Coulomb's friction law which is quite suitable to steel elements [21].

Among the elements available in the ABAQUS code, able to model the interaction between two bodies, the contact element which allows the finite sliding interaction between a deformable and a rigid body has been considered for these applications. In particular, this element embodies kinematic measures of overclosure and relative shear sliding together with an appropriate Lagrange multiplier technique to enforce contact. Separation and sliding of finite amplitude and arbitrary rotations may be modeled and an isotropic Coulomb friction model and are adopted to reproduce friction conditions.

3.4. Bolt modeling

In general, bolts behave in a 3D fashion in connections. Hence, they have been modeled in the benchmarks *T*1 [see Fig. 3(a)] by means of JET3D elements [19]. Nevertheless, to reduce the number of contact planes, washers have been considered attached to bolt heads whilst bolts have been assumed to be symmetric. To comply with these assumptions, the additional flexibilities provided by the nut and the threaded part of the shank have been incorporated into an effective bolt length according to Agerskov's model [26]. That model is based on the following equation:

$$\frac{EA_b}{K_1+2K_4}=\frac{B}{\Delta l_b}=\frac{EA_s}{L_{eff}} \tag{1}$$

in which A_b and A_s indicate the gross cross-section and the tensile stress area, respectively, B and Δl_b define the bolt force and the corresponding bolt elongation whilst the effective length L_{eff} is unknown. K_1 and K_4 are parameters which can be obtained readily from the bolt geometry illustrated in Fig. 6. In detail, the following relations hold:

$$K_1 = l_s + 1.43l_t + 0.71l_n,\ K_4 = 0.1l_n + 0.2l_w. \tag{2}$$

By remarking that the threaded part of the bolt shank triggers off tensile yielding and failure, the bolt shank is reproduced with a cylinder of cross-section area A_s. By means of this assumption, L_{eff} can be obtained readily from Eq. (2). A typical bolt discretization is illustrated in Fig. 7(a). However, to avoid such a complicated 3-D finite element mesh, a beam assemblage, labeled *spin*, was conceived by Bursi and Jaspart [27]. This model can be observed in Fig. 7(b).

To validate the *spin* model, separate simulations were conducted for the bolt shank and the bolt head. In particular, isolated 8.8 grade M 12 bolts were analyzed [27]. Thereby, a bolt shank length of 20 mm which takes into account both washer and nut flexibilities according to Agerskov's proposal, [26] was considered. Numerical simulations were carried out either with 3-D solid elements by means of the LAGAMINE code or with the spin model proposed in Fig. 7(b). Shank simulations were performed by subjecting the bolt shank to combined tensile and flexural stresses through the bolt head. Only results related to the ratio M/N equal to 2 mm are presented here. The evolution of axial displacement *vs* the axial force at the shank top and the corresponding moment-rotation (M–φ) relationships are shown in Fig. 8(a) and 8(b), respectively. One can observe how at least two beam elements are necessary to capture the actual stiffness and strength behaviour of a 3-D bolt shank with satisfactory accuracy.

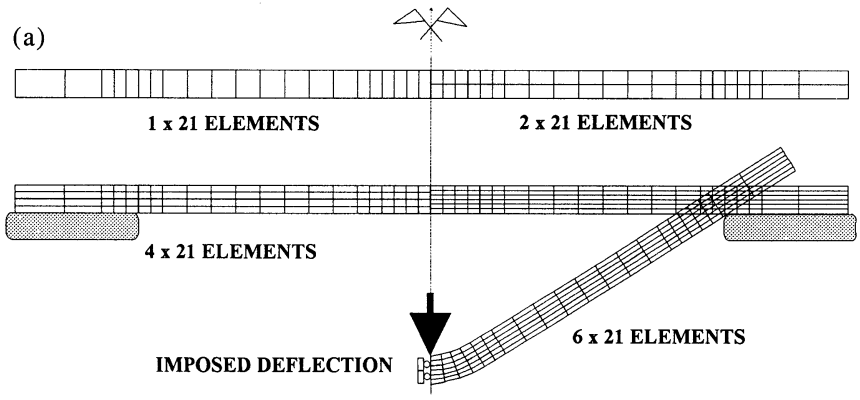

Fig. 5a. *Caption opposite*

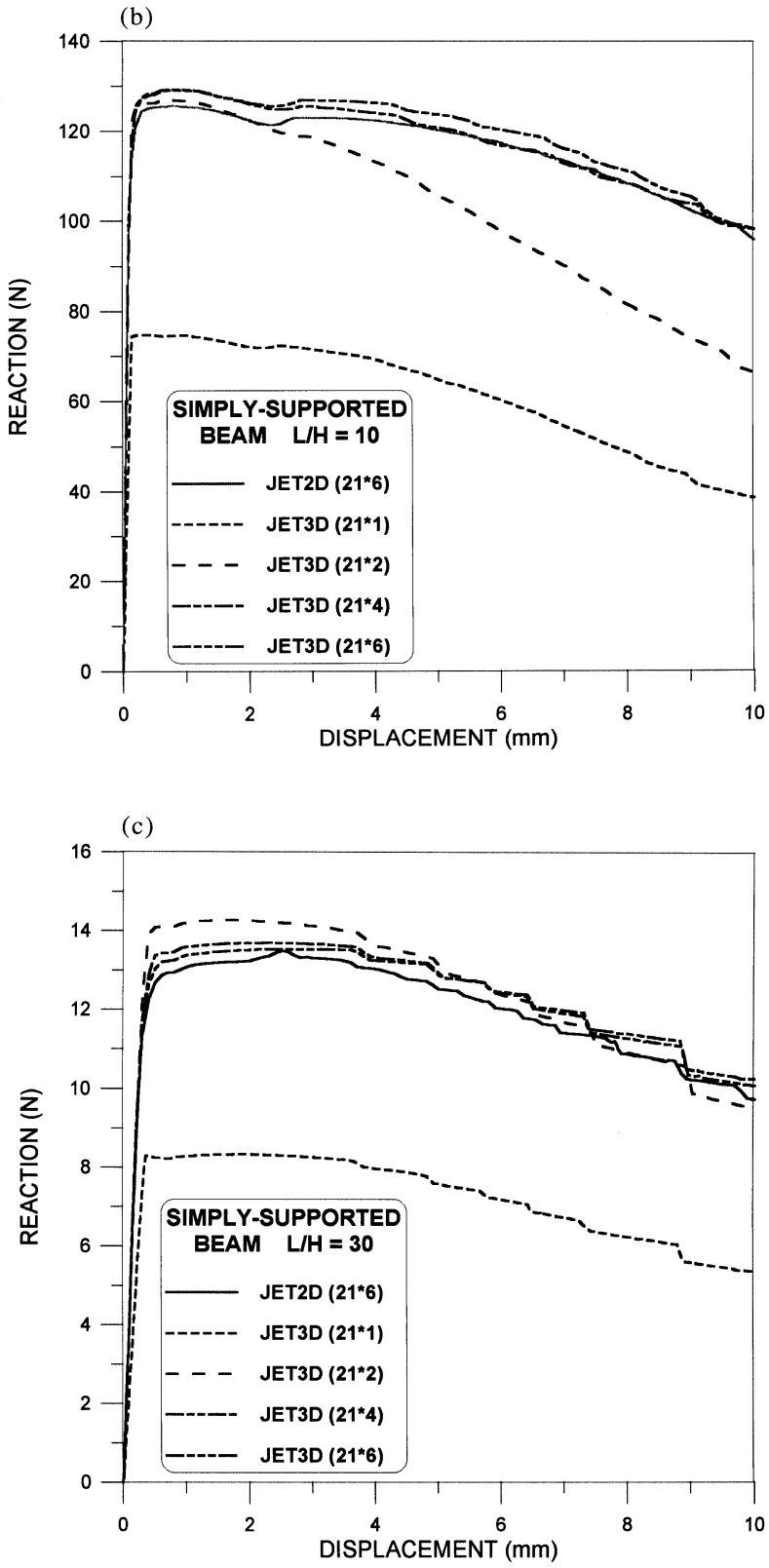

Fig. 5. Simply-supported beam with an imposed central defection [18]: (a) FE idealizations; (b) simulations for a slenderness ratio $L/H = 10$; (c) simulations for a slenderness ratio $L/H = 30$.

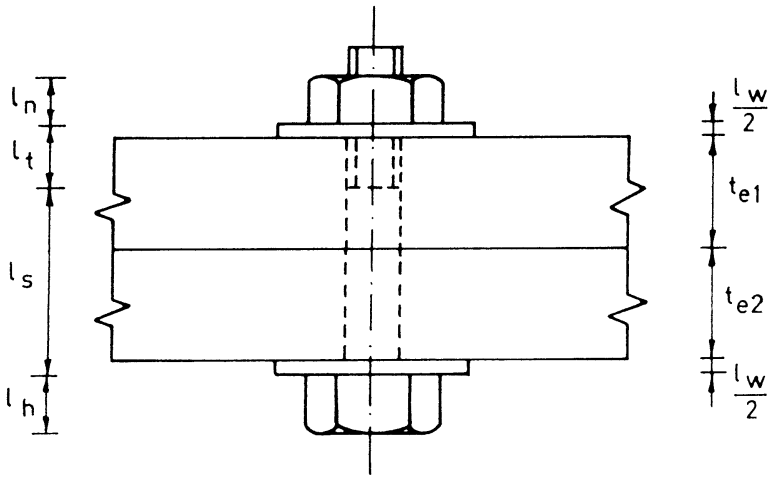

Fig. 6. Bolt geometry adopted in Agerskov's model [26].

The beam sections adopted to reproduce the bolt head [see Fig. 7(b)] were calibrated with finite element analyses by subjecting the 3-D bolt head shown in Fig. 7(a) to combined bending and shear. Thereby, two sets of beams were determined [see Fig. 7(b)] to embody the restraining effect of the bolt shank. As a viable and simple alternative, beam sections were also computed analytically on the basis of the actual bolt head geometry. In particular, the inner beams were assumed to have flexural and shear stiffnesses four times larger than the relative stiffnesses of the outer beams. Simulations performed on both benchmarks *T*1 and *T*2 by using both assumptions demonstrated the feasibility of the simplest model in reproducing bolt head effects.

3.5. Kinematic descriptions

The kinematic descriptions adopted in both LAGAMINE and ABAQUS codes allow finite element ana-

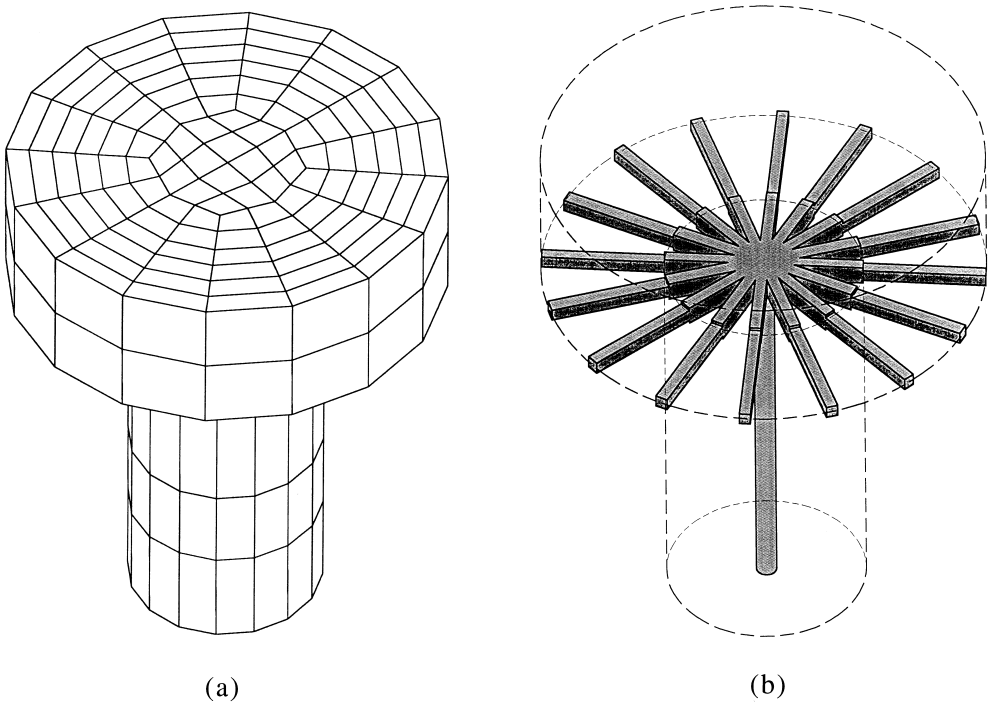

Fig. 7. Bolt FE idealization: (a) 3-D continuum model; (b) spin model.

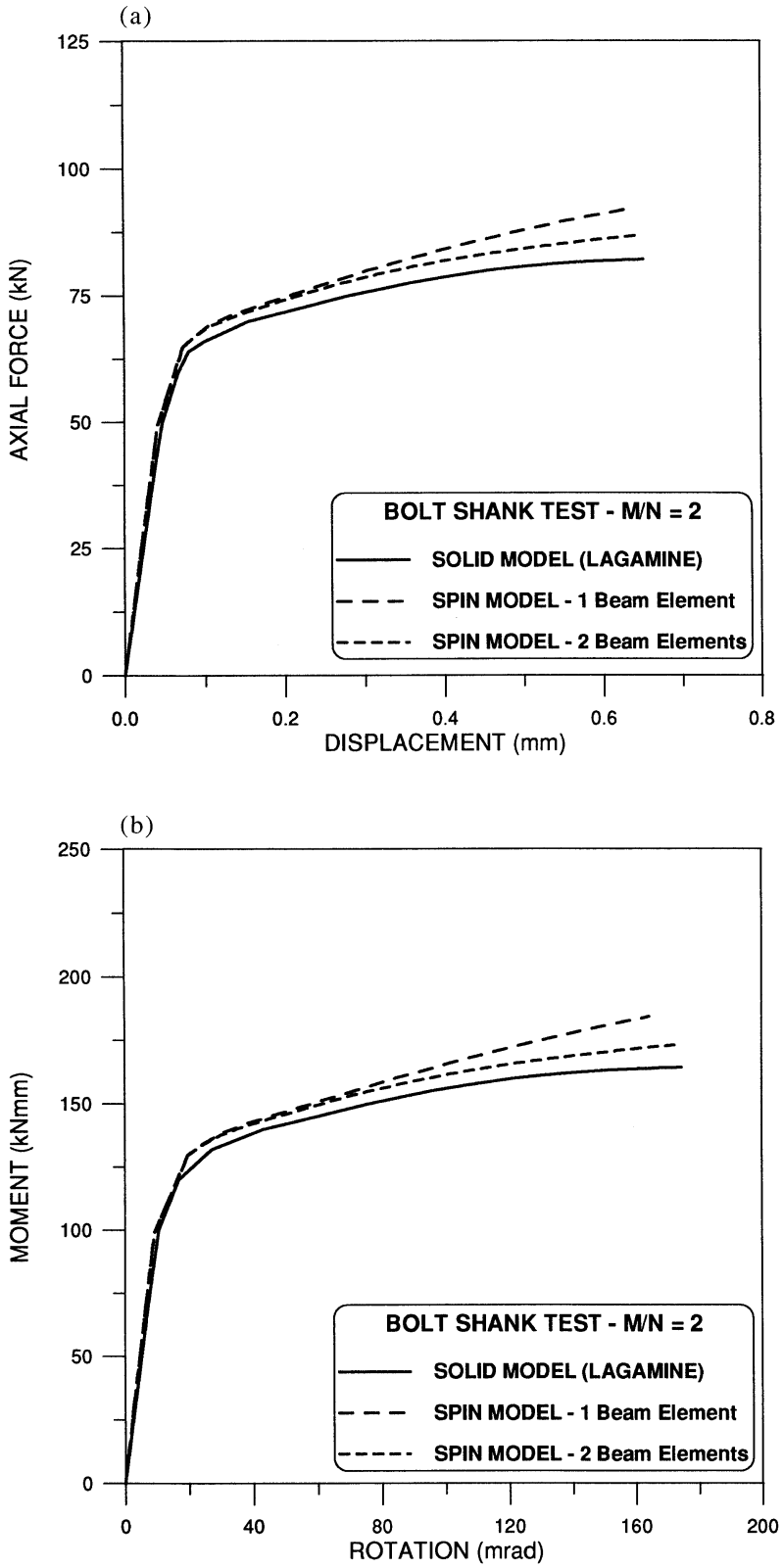

Fig. 8. Comparison between the continuum FE mesh and the spin FE model for $M/N = 2$: (a) shank top displacement vs axial force; (b) shank top rotation vs bending moment.

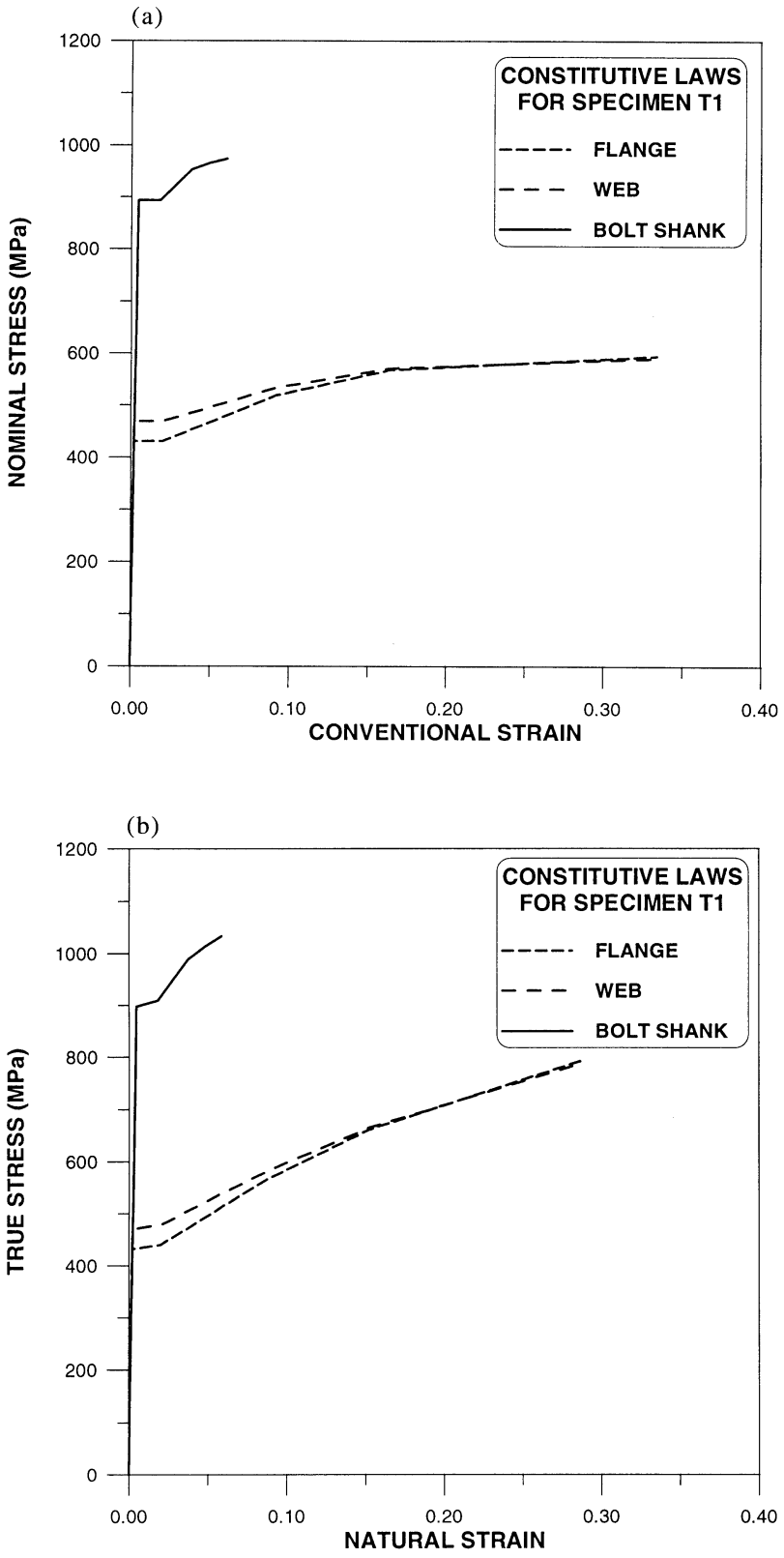

Fig. 9. Piecewise linear stress–strain relationships of tee stub *T*1: (a) nominal law; (b) true law.

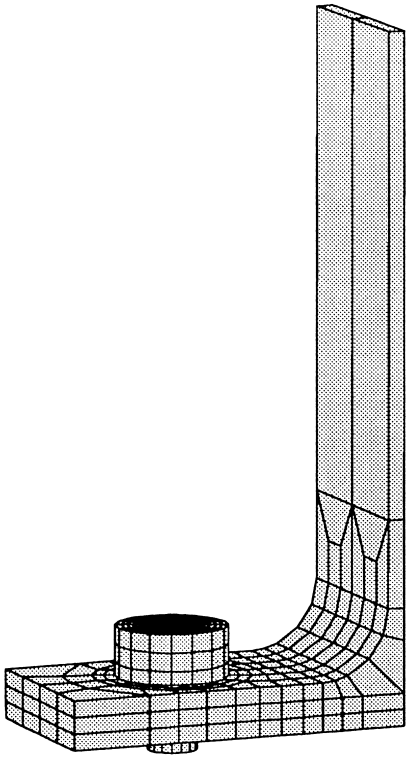

(a)

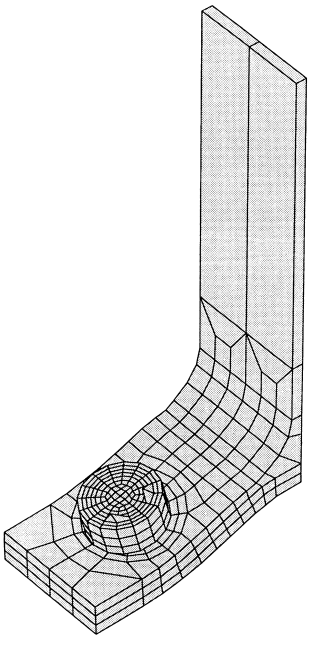

(b)

Fig. 10. FE idealization of preloaded tee stub connection *T*1: (a) undeformed mesh; (b) displacement field at the plastic failure state.

lyses with large displacements, large rotations and large strains to be performed. These features are deemed necessary to trace both the connection behaviour in the post-failure regime and membrane effects in thin connecting elements [7].

The kinematic descriptions of hexahedra and contact elements in LAGAMINE for geometrically non-linear finite element analyses are based on an updated Lagrangian Jaumann (ULJ) and a corotational (CR) formulation, respectively. In the ULJ formulation, the last target configuration, once reached, becomes the next reference configuration. Strain and stresses are redefined as soon as the reference configuration is updated [28]. The equations in the ULJ description are much simpler than those in the total Lagrangian description (TLD) because all the non-linear contributions of the discretized displacement field vanish. In the CR formulation, two reference configurations are adopted. Strains are measured from the corotated configuration whereas the base configuration is maintained as a reference for measuring rigid body motions.

In a large deformation analysis, appropriate strain and stress measures have to be adopted to deal with the continuous change of both configuration and volume of the body. Thereby, the velocity strain and the Jaumann stress rate [28], which are conjugate in a virtual work sense, are used in the hexahedron formulation [29]. On the other hand, the CR formulation requires the rate of deformation and both the normal and tangential contact stresses as energetically conjugate strain–stress measures [21].

The corresponding kinematic descriptions for geometrically non-linear finite element analyses in ABAQUS are based on a sort of updated Lagrangian formulation. In this formulation, the reference configuration is assumed to be the natural elastic state of the body, *viz*. the state to which the body returns upon unloading. The appropriate strain and stress measures are the rate of deformation and the corotational rate of Kirchhoff stress which are conjugate in a virtual work sense [28]. It can be proved that this stress rate is objective under superimposed rigid body motions.

3.6. Material properties, constitutive integration and yield criterion

In order to perform realistic simulations, actual material properties are required. Thereby, main material data for flanges, webs and bolt shanks collected in Tables 3 and 4 are reproduced with piecewise linear constitutive laws of the type illustrated in Fig. 9. The plot of Fig. 9(a), which is relevant to specimens *T*1, represents conventional strains and nominal stresses, defined as the change in length per unit initial length and as the axial force per unit initial area of the cross section, respectively. Because both the LAGAMINE and

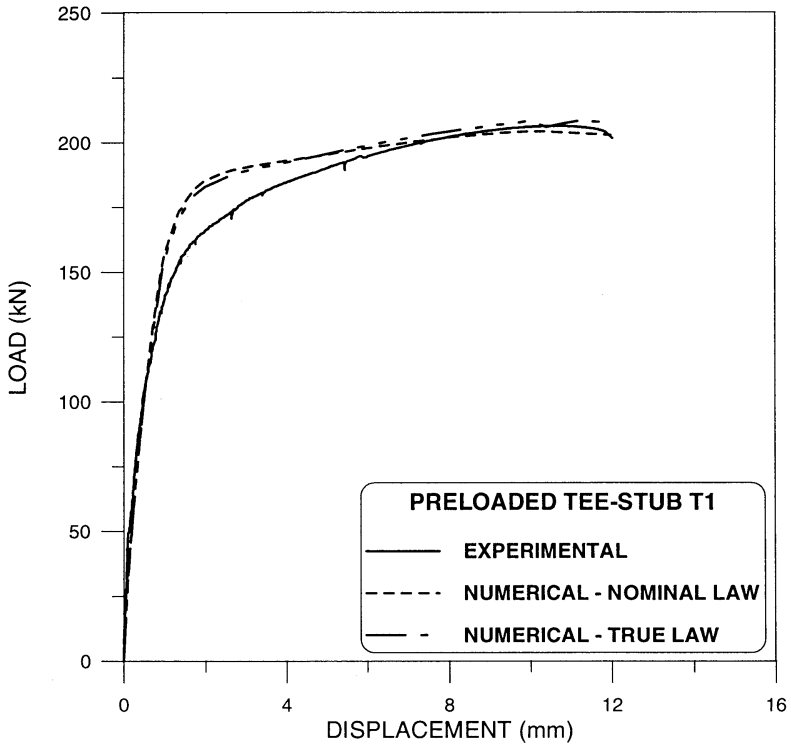

Fig. 11. Experimental and predicted relative displacement Δd vs load F of the preloaded tee stub $T1$.

the ABAQUS code operate in a large deformation setting, natural strain-true stress curves are required for a proper definition of the uniaxial material response [28]. These quantities are defined with respect to the current value of length and cross-sectional area, respectively, and can be obtained readily by means of the following

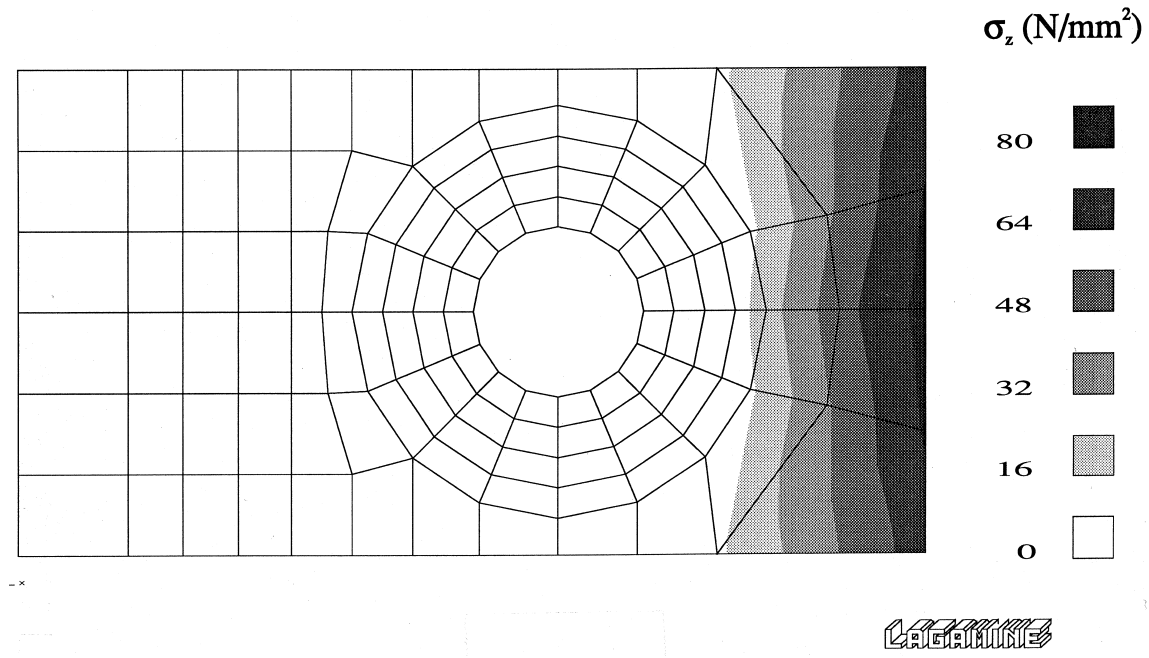

Fig. 12. Normal pressure distribution at the plastic failure state of the preloaded tee stub $T1$.

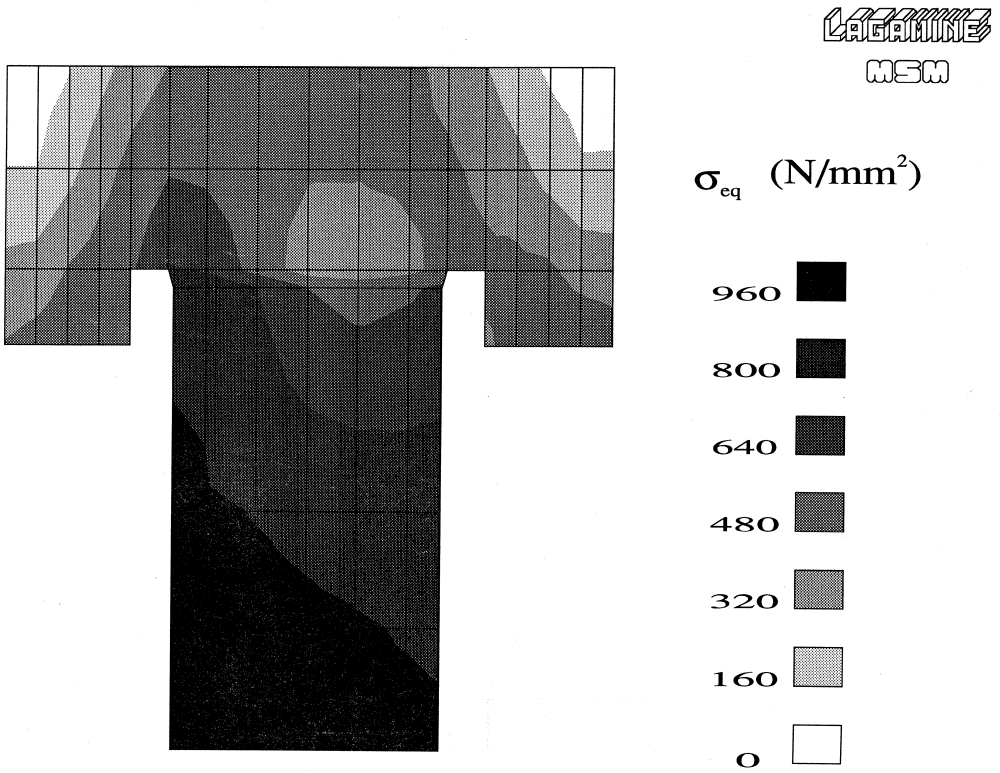

Fig. 13. von Mises equivalent stress field of bolt at plastic failure state in the preloaded tee stub *T*1.

equations:

$$\epsilon = \ln(1+e),\ \sigma = s(1+e) \tag{3}$$

if plastic deformations are assumed to occur at constant volume. In detail, e represents the conventional strain, ϵ is the natural strain, s defines the nominal stress and, finally, σ denotes the true stress. The conversion outcome performed by means of Eq. (3) on the stress–strain curve represented in Fig. 9(a) is provided in Fig. 9(b).

The numerical integration of constitutive relationships is performed both by LAGAMINE and ABAQUS codes with a robust radial return mapping algorithm which gives exact results for piecewise linear hardening material. Thereby, the finite element solution accuracy is not governed by the size of the integration step. Finally, the well known Huber–Mises–Hencky yield criterion is used to reproduce the ductile yielding of steel elements.

4. Finite element results for tee stub connections

The finite element model adopted to reproduce a quarter of the tee-stub connection reflects the assumptions and conclusions derived in previous sections. It is illustrated in Fig. 10(a) for specimen *T*1. The model embodies three elements along the thickness whilst elements are concentrated where high stresses and strain discontinuities, *viz*. the yield lines, are likely to occur. No friction has been assumed between the bottom flange and the rigid foundation because of the symmetric behaviour of specimens. However, a friction coefficient $\mu = 0.25$ has been adopted at the bolt head–flange interface. As mentioned in a previous section, the bolt head incorporates the washer and its shank length including the flexibility effects both of the threaded part and the nut. Preloading forces are applied as initial stresses.

The displacement field at the plastic failure state traced by the finite element analysis is illustrated in Fig. 10(b) for the preloaded specimen *T*1. One can observe how the model is able to reproduce the flange kinematics and the relative movement between flange and bolt head. The accuracy of the finite element model can be quantified by superimposing the computed load–displacement (F–Δd) relationships upon the measured one, as illustrated in Fig. 11. In detail, F defines the applied external load whilst Δd indicates the variation of d [see Fig. 3(a)]. The two simulations refer to the adoption of the conventional strain–nominal stress law depicted in Fig. 9(a) and the natural

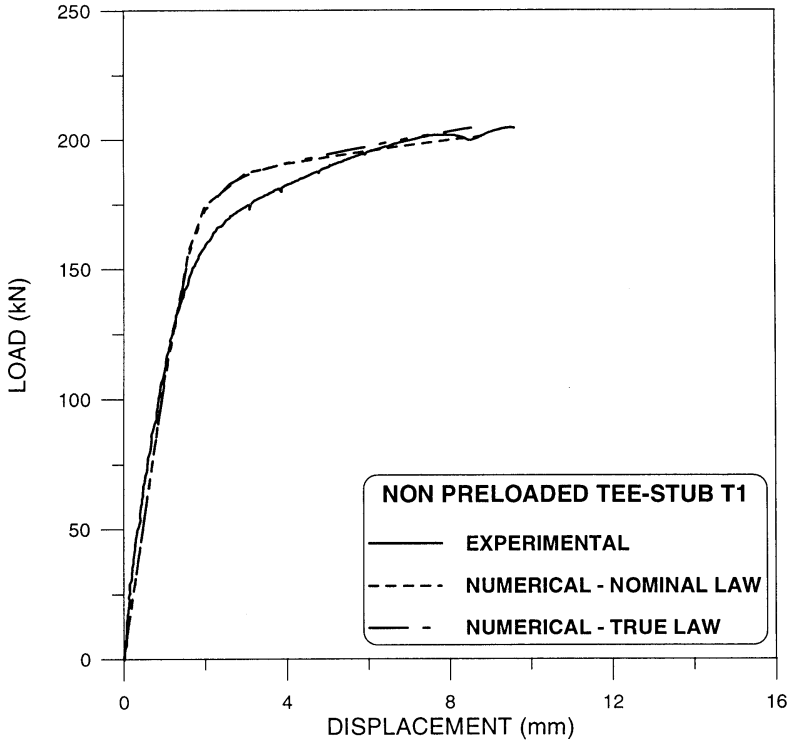

Fig. 14. Experimental and predicted relative displacement Δd vs load F of the nonpreloaded tee stub $T1$.

strain–true stress law illustrated in Fig. 9(b), respectively. From the comparison, one can observe the good accuracy of both simulations. Some discrepancies are only evident at the onset of yielding, due to residual stress effects, which determine a more gradual plastification of the specimen, and which are disregarded in the model due to lack of data. As expected, the simulation based on the natural strain–true stress law is slightly more accurate in the inelastic range. However, the specimen zone subjected to large deformations is rather limited and, therefore, only the results based on the conventional strain–nominal stress law are commented upon.

Once the finite element model is proved to be reliable, it can be adopted to generate information which cannot be provided from tests. For example, significant data can be obtained by plotting contact pressures developed between tee-stub flanges. Fig. 12 highlights the normal pressure distribution at the plastic failure state in the external part of the tee-stub. This distribution can be used to quantify the location and amplitude of prying forces. The model can also provide detailed information on bolt behaviours. The evolution of von Mises stresses in each bolt and washer can be observed at the plastic failure state of the tee stub in Fig. 13. Yielding can be observed in the bolt shank, indicating that bolts also participated in the plastic failure mechanism to a certain extent.

For brevity, the accuracy of the finite element model for the corresponding non-preloaded specimen, $T1$, is assessed by comparing the load–displacement (F–Δd) relationships shown in Fig. 14. Also for this case, a major discrepancy can be observed at the onset of yielding, in which the actual plastification appears to be more gradual due to the residual stress effects. Additional results can be found in Bursi and Jaspart [8].

For conciseness, the accuracy of the *spin* model, proposed in Section 3.4, is assessed here by simulating the elastic–plastic behaviour of benchmark $T1$ only. The continuum is modeled by means of C3D8 bricks, or, as an alternative, by means of C3D8I and C3D8R bricks of the ABAQUS library. The contact elements, with finite sliding and finite rotation capabilities, were adopted to reproduce the friction conditions in the bottom part of the flange. A friction coefficient $\mu = 0$ was adopted to comply with the benchmark symmetry requirements. The bolt was reproduced through the *spin* model illustrated in Fig. 7(b), by adopting 16 beams for the inner part and the same number of beams for the outer part of the bolt head. However, only five elements were adopted to discretize the bolt shank. The beam element adopted in the finite element model is labeled $B31$ [15].

The displacement field at the plastic failure state, traced by the finite element analysis, is illustrated in Fig. 15(a). One can observe how the model is able to

reproduce the complex displacement field of the specimen. The computed load–displacement (F–Δd) relationships are compared to the measured one as well as to the LAGAMINE simulation in Fig. 15(b). A good performance of the models can be observed, apart from the discrepancies at the onset of yielding due to residual stress effects. However, C3D8I elements behave particularly well in the inelastic range, being purposely designed for bending-dominated problems. As expected, C3D8R elements underestimate the plastic failure load, whilst the prediction with C3D8 elements appears to be unsatisfactory, owing to the overestimation of the plastic failure load. This is a negative effect caused by the shear locking phenomenon.

The corresponding simulations for the non-preloaded specimen, $T1$, are illustrated in Fig. 15(c). One can observe the good performance of C3D8I elements both in the elastic and inelastic regimes. The locking effect embodied in the response based on C3D8 elements is evident.

Finally, the accuracy provided by the spin bolt model incorporated in the preloaded tee stub, $T1$, is estimated comparing the relevant bolt axial force–applied total force traced by the model in Fig. 16. One can observe how the spin model can capture the evolution of the bolt force with a satisfactory accuracy.

5. Finite element results for end plate connections

It is evident from the results collected in Table 2 that the extension of the end plate on both sides of the beam flanges does not influence significantly the stiffness and strength characteristics of EPB specimens compared to those of EP specimens. As a result, finite element analyses presented here are restricted to EP connections. In addition, only the limiting case of a thin end plate connection with a thickness $t_p = 12$ mm is considered. Indeed, this connection was endowed with a complex 3-D failure kinematic mechanism and,

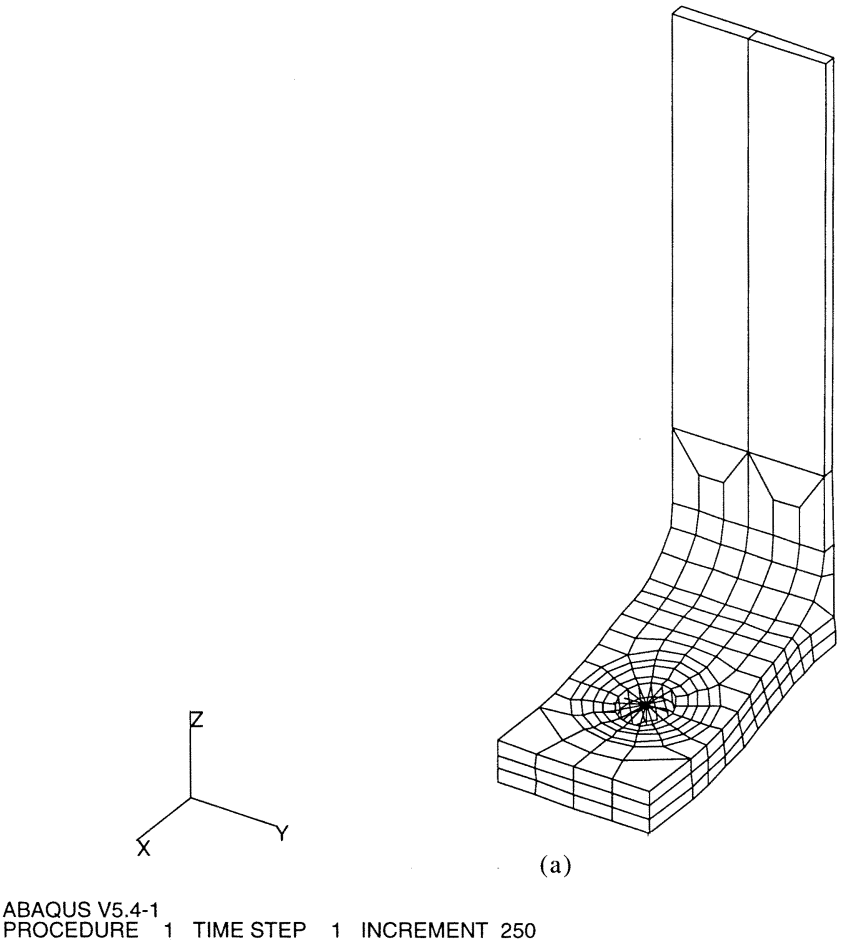

Fig. 15a. *Caption on next page*

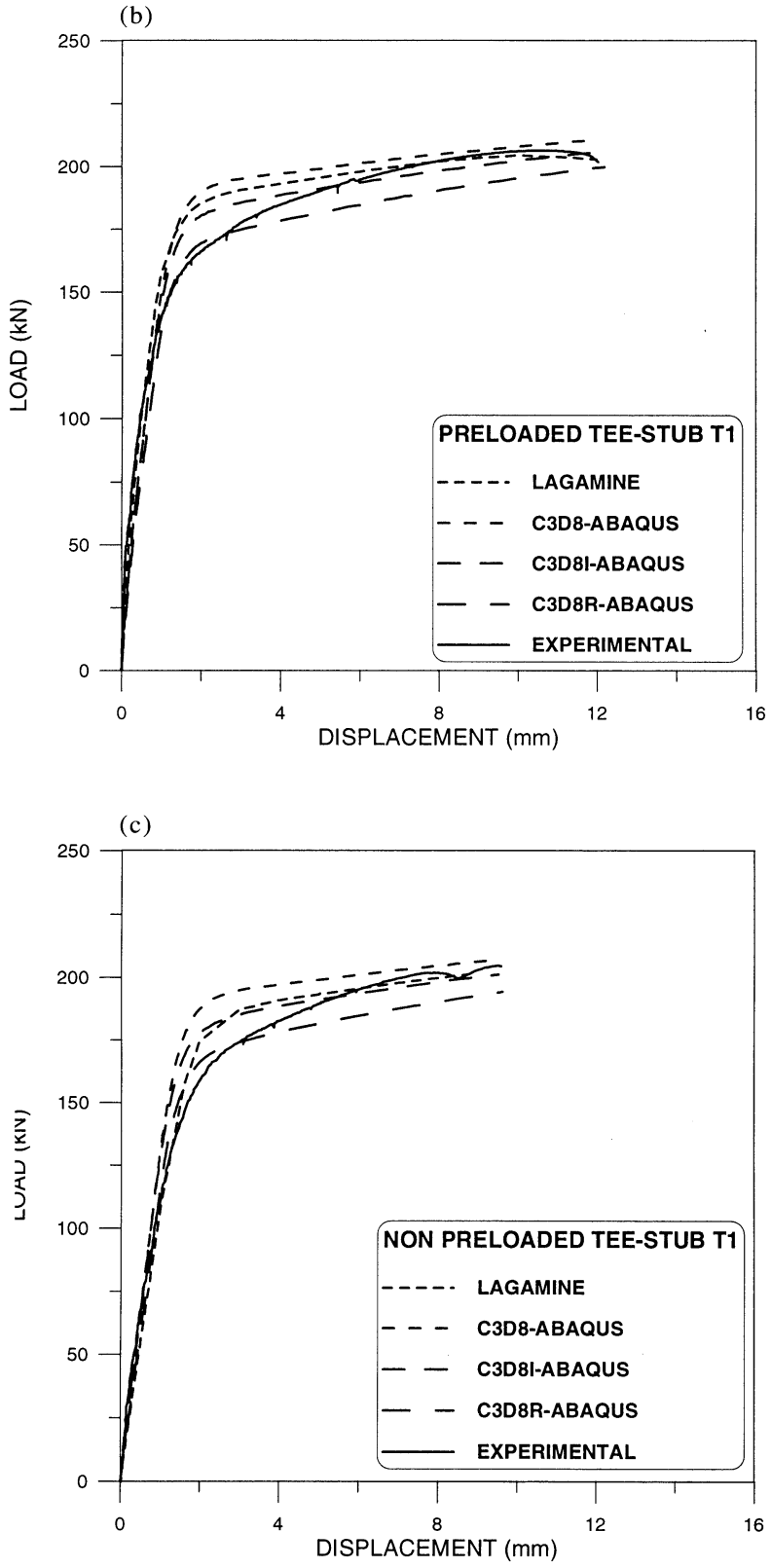

Fig. 15. (a) Displacement field at the plastic failure state of the preloaded tee-stub $T1$; (b) experimental and predicted relative displacement (F–Δd) relationship; (c) experimental and predicted (F–Δd) relationship for non-preloaded tee-stub $T1$.

therefore, it represents a severe test for finite element analysis [17].

The geometrical characteristics of this connection, labeled EP 1–1, are illustrated in Fig. 1(b) whilst the mechanical characteristics are collected in Table 3. Bolt shanks M 20 are discretized by means of 11 B31 elements [15] whilst two sets of 18 inner and outer beams have been adopted to model the bolt head, respectively. Only bolts in the end plate tension zone have been modeled. The end plate mesh encompasses the features of the previous tee stub discretization and it is characterized by three finite element layers within the thickness. Also, weld beads have been modeled by means of 6-node linear triangular C3D6 elements [15]. The complete model embodies 3684 elements and 19,600 nodes. The piecewise linear constitutive laws for the material are reproduced in Fig. 17(a). Only nominal strain–conventional stress laws are considered in the following simulations owing to the limited influence of the true law on the connection response. The isotropic Coulomb friction criterion with a mean value of $\mu = 0.25$ is adopted in these simulations. In addition, consistent nodal forces are applied to tension and compression beam flanges to simulate the applied flexural action.

The displacement field at the plastic failure limit state, traced by the analysis, is reported in Fig. 17(b). The model appears very accurate in reproducing the complex kinematics dominated by bending around the plate tension zone [7]. The moment–rotation (M–φ) relationship determined by the finite element model with different ABAQUS brick elements is superimposed upon the corresponding experimental curve in Fig. 17(c). From this figure, it is clear that the model constituted by C3D8I elements approximates, with good accuracy, the measured moment–rotation curve. Indeed, the end plate behaviour is governed mainly by bending stresses. Lack of fit phenomena, imperfections and residual stresses determine, however, the observed discrepancies up to the onset of yielding. At the ultimate limit state, the simulation is also able to reproduce membrane effects which did not developed completely during testing, owing to a premature buckling of the compressed beam flange [7]. The corresponding simulation performed with C3D8 elements mirrors their inadequacy to reproduce bending-dominated problems whilst, as expected, C3D8R elements underestimate consistently the connection strength. Friction effects on the connection response can be assessed more strictly from Fig. 17(d), in which friction coefficient limiting values ranging from 0.0 to 0.5 have been considered. As expected, these effects are rather limited on the connection rotational response.

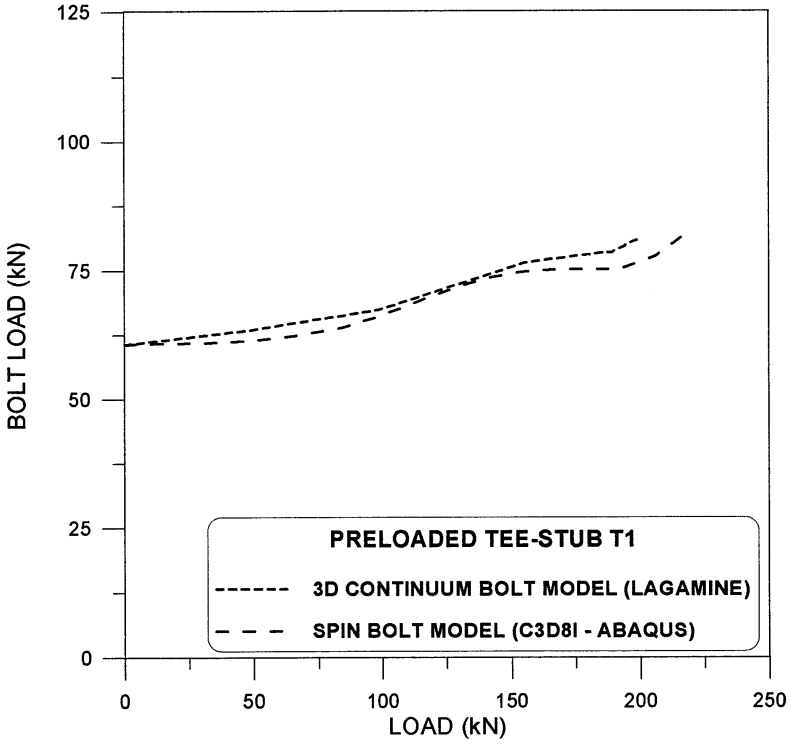

Fig. 16. Predicted bolt axial force vs total force F from the 3-D continuum and the spin model.

6. Concluding remarks

In this contribution, an attempt has been made to provide an overview of current developments for estimating the moment–rotation behaviour of bolted moment resisting connections and to establish a legitimate methodology for finite element analysis of extended end plate connections. In detail, the calibration of finite elements of the commercial code ABAQUS on test data of elementary tee stub connections as well as simulations provided by the LAGAMINE code were initially performed to scrutinize issues related to discretization, element types, kinematic descriptions, constitutive relationships and step size. Next, an assemblage of three-dimensional beam finite elements, *viz*. the *spin*, was proposed to model the bolt behaviour in a simplified yet accurate fashion. Lastly, a proper three-dimensional non-linear finite element model suitable to the analysis of extended end plate moment resisting steel connections was proposed and validated.

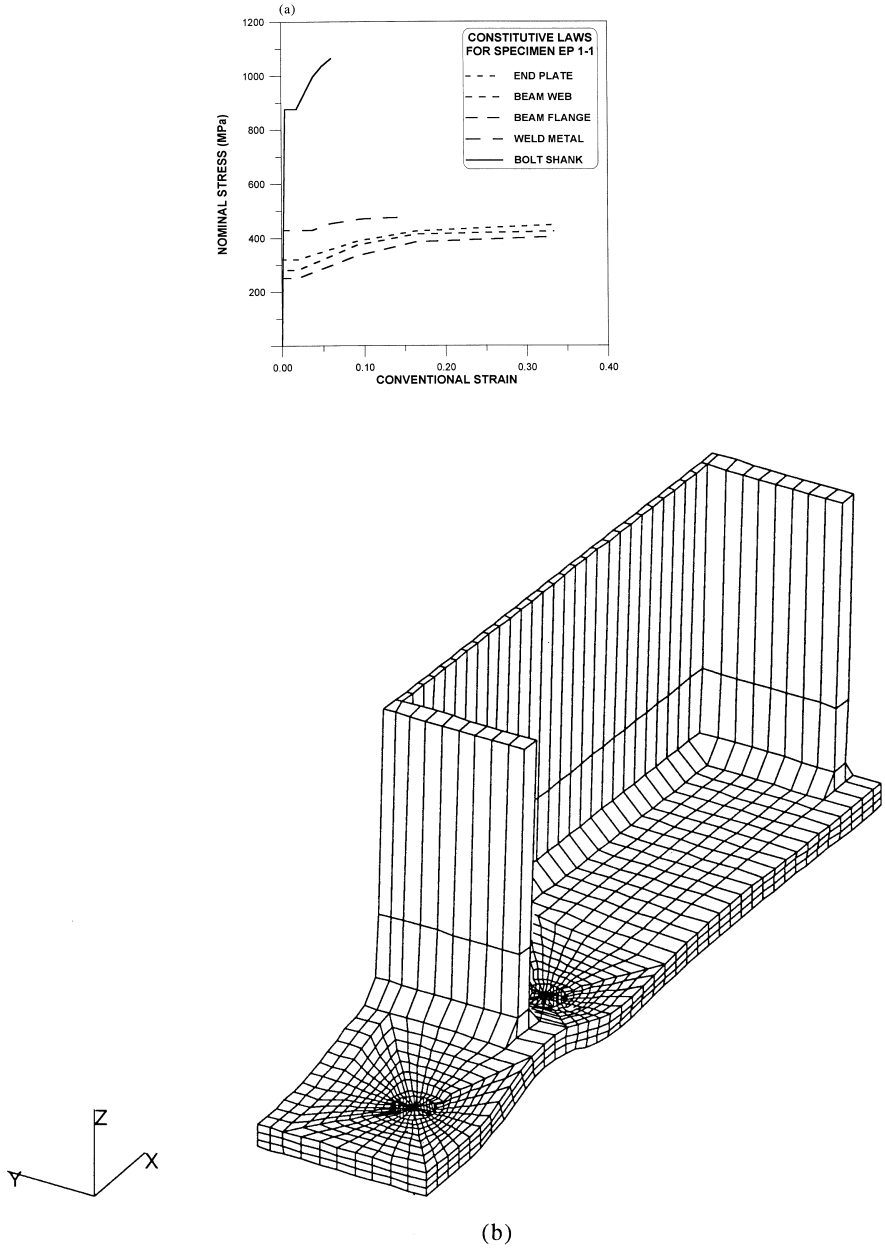

Fig 17a–b. *Caption opposite*

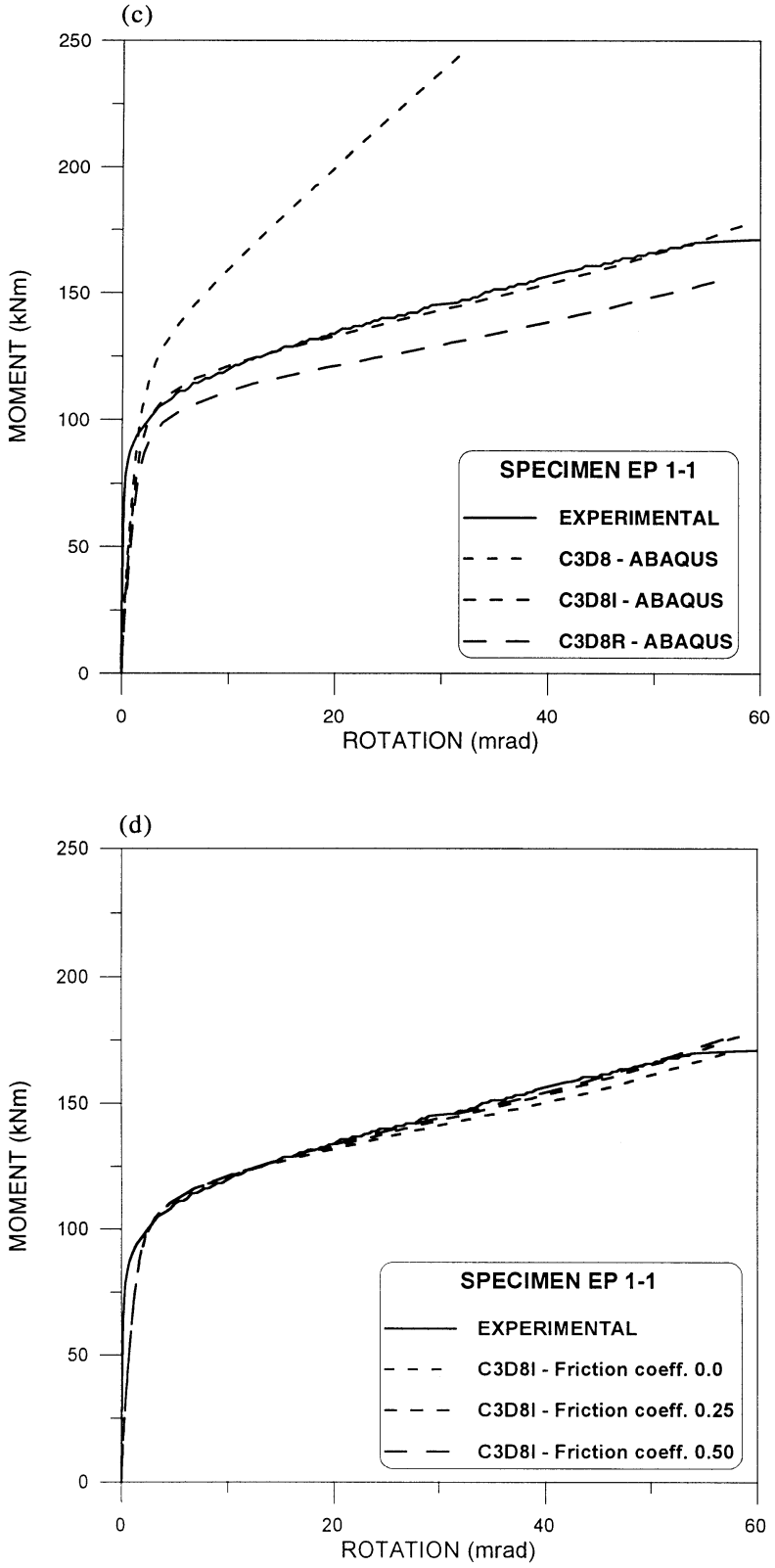

Fig. 17. Extended end plate connection EP 1–1: (a) nominal piecewise linear stress–strain relationships; (b) displacement field at the plastic failure state; (c) experimental and predicted rotation φ vs applied bending moment M; (d) friction effects.

Acknowledgements

The work reported in this paper is granted by MURST of Italy. Specific support to the Universities of Trento and Liege were also provided by the SPRINT Contract RA 351 financed project "Steel and composite building frames using semi-rigid connections: from research to design practice". The findings, observations and conclusions in this paper are, however, those of the writers.

References

[1] American Institute of Steel Construction. Manual of steel construction—load and resistance factor design. 1st ed. Chicago, 1986.
[2] Eurocode 3. Design of steel structures part 1.1: general rules and rules for buildings, ENV 1993-1-1. Brussels, 1992.
[3] American Institute of Steel Construction. Extended end-plate moment connections, steel design guide S. Chicago, 1990;4.
[4] Eurocode 3. New revised annex J: joints in building frames, ENV 1993-1-1/pr A2. Brussels, 1994.
[5] Bernuzzi C, Zandonini R, Zanon P. Rotational behaviour of end-plate connections. Costr. Metal. 1991;2:3–32.
[6] Krishnamurthy N. A fresh look at bolted end-plate behavior and design. Engng J, AISC 1978;15(2):39–49.
[7] Bursi OS. An experimental–numerical method for the modelling of plastic failure mechanisms of extended end plate steel connections. Struct Engng Rev 1991;3:111–9.
[8] Bursi OS, Jaspart JP. Benchmarks for finite element modelling of bolted steel connections. J Constr Steel Res 1997;43(1–3):17–42.
[9] Krishnamurthy N, Graddy D. Correlation between 2 and 3-dimensional finite element analysis of steel bolted end-plate connections. Comput Struct 1976;6:381–9.
[10] Kukreti AR, Murray TM, Abolmaali A. End plate connection moment–rotation relationship. J Constr Steel Res 1987;8:137–57.
[11] Kukreti AR, Murray TM, Ghassemieh M. Finite element modeling of large capacity stiffened steel tee-hanger connections. Comput Struct 1989;32(2):409–22.
[12] Chasten CP, Lu LW, Driscoll GC. Prying and shear in end plate connection design. J Struct. Engng 1992;118(5):1295–311.
[13] Sherbourne AN, Bahaari MR. 3-D simulation of end-plate bolted connections. J Struct Engng 1994;120(11):3122–36.
[14] Gebbeken N, Rothert H, Binder B. On the numerical analysis of end plate connections. J Constr Steel Res 1994;30:177–96.
[15] ABAQUS—user's manual. 1994. vols 1 and 2, version 5.4. Pawtreket, RI: Hibbitt, Karlsson & Sorensen.
[16] ABAQUS—theory manual. 1994. Version 5.4. Pawtreket, RI: Hibbitt, Karlsson & Sorensen.
[17] Bursi OS, Leonelli L. A finite element model for the rotational behavior of end plate steel connections. In: Proc. SSRC Annual Technical Session. Chicago, 1994:163–75.
[18] Li KP. Contribution to the numerical simulations of three-dimensional sheet forming by finite element method, chapter 2. Ph.D. thesis. MSM, University of Liege, Belgium, 1996.
[19] Li KP, Cescotto S, Jetteur P. An element with hourglass control for large deformation analysis in three dimensions. In: Proc Third Int Conf on Computational Plasticity: Fundamentals and Applications, Barcelona, 1992:2021–32.
[20] Jetteur P, Cescotto S. A mixed finite element for the analysis of large inelastic strains. Int J Num Meth Engng 1991;31:229–39.
[21] Charlier R, Habraken AM. Numerical modellisation of contact phenomena by finite element method. Comput Geotech 1990;9:59–72.
[22] Cescotto S, Habraken A-M, Radu JP, Charlier R. Some recent developments in computer simulations of metal forming processes. In: Proc 9th Int Conf on Computer Methods in Mechanics. Krakow–Rytro, Poland, 1989:19–52.
[23] Belytschko T, Fish J, Engelmann BE. A finite element with embedded localization zones. J Comput Meth Appl Mech Engrg 1988;70:59–89.
[24] Flanagan DP, Belytschko T. A uniform strain hexahedron and quadrilateral with orthogonal hourglass control. Int J Num Meth Engng 1981;17:679–706.
[25] Simo JC, Rifai MS. A class of assumed strain methods and the method of incompatible modes. Int J Num Meth Engng 1990;29:1595–638.
[26] Agerskov H. High-strength bolted connections subject to prying. J Struc Engng Div, ASCE 1976;102(1):161–75.
[27] Bursi OS, Jaspart JP. Calibration of a finite element model for bolted end plate steel connections. J Constr Steel Res 1997;44(3):225–62.
[28] Bathe KJ. Finite element procedures in engineering analysis. Englewood Cliffs, NJ: Prentice-Hall, 1982.
[29] Cescotto S, Habraken A-M. Numerical modellisation of contact phenomena by the finite element method. Comput Geothec 1990;9:59–72.